Chinese Chemical Letters 35 (2024) 109430

Contents lists available at ScienceDirect

Chinese Chemical Letters

journal homepage: www.elsevier.com/locate/cclet

# Highly efficient and photothermally stable CDs@ZIF-8 for laser illumination

Zhi Wang[a], Lingpeng Yan[a,b], Yelin Hao[a], Jingxia Zheng[a], Yongzhen Yang[a,*], Xuguang Liu[a,b]

[a] Key Laboratory of Interface Science and Engineering in Advanced Materials, Ministry of Education, Taiyuan University of Technology, Taiyuan 030024, China

[b] College of Materials Science and Engineering, Taiyuan University of Technology, Taiyuan 030024, China

ARTICLE INFO

*Article history:*
Received 3 November 2023
Revised 13 December 2023
Accepted 18 December 2023
Available online 24 December 2023

*Keywords:*
Carbon dots
Metal-organic frameworks
High photothermal stability
High photoluminescence quantum yield
Laser illumination

ABSTRACT

Carbon dots (CDs), as a solid-state phosphor, have great potential for application in a new solid-state lighting device—laser diode (LD). For high efficiency LD devices, both high photoluminescence quantum yield (PLQY) and high photothermal stability of CDs are essential. Herein, yellow CDs@ZIF-8 composites with high structural stability were prepared by encapsulating CDs in zeolitic imidazolate framework-8 (ZIF-8) through electrostatic adsorption between CDs and ZIF-8, in which CDs with amino groups on the surface were used as luminescent feeders and ZIF-8 was used as a protective layer matrix. The as-prepared CDs@ZIF-8 not only possess a high PLQY of up to 81.17%, but also maintain a high fluorescence intensity of 100% and 80% under long-term illumination (60 min) and high temperature (478 K), respectively. The hydrogen bonding between CDs and ZIF-8 in the encapsulated structure can enhance the degree of electron cloud delocalization, which can improve the PLQY of CDs@ZIF-8. Meanwhile, CDs@ZIF-8 has high photothermal stability due to the binding effect of ZIF-8 on CDs and high thermal stability of ZIF-8. The white LD device, fabricated from CDs@ZIF-8 as a phosphor in combination with 450 nm blue LD, has a color coordinate of (0.37, 0.33), a color temperature of 3762 K, and a high color rendering index of 86. This study provides a new strategy for the construction of solid-state phosphors with high PLQY and high photothermal performance.



Laser diode (LD), as a new type of solid-state lighting device, has the advantages of higher luminous efficiency, longer visible light distance, faster response speed and no "efficiency droop" phenomenon compared with light emitting diode (LED). LD has attracted much attention in the fields of automobile headlights, searchlights, endoscopes, projectors and laser televisions [1–3]. At present, white laser diode (WLD) is mostly realized by blue LD to excite yellow fluorescence conversion materials, which mainly are rare earth doped phosphors with good stability and mature synthesis process [4]. However, the high cost and complex preparation process of rare earth doped phosphors dramatically restrict their further application and development.

Carbon dots (CDs) can be used as a new type of phosphor for LD illumination to construct non-toxic and low-cost LD devices because they possess the benefits of tunable emission wavelength, good light stability, and simple synthesis [5–10]. In 2015, Feng *et al.* [11] embedded CDs and lanthanide complexes into polymethyl methacrylate to produce a white light polymer composite film for LD illumination, pioneering the use of CDs in LD illumination application. In 2018, Qu *et al.* [12] treated blue CDs with hydrogen peroxide to obtain green solid-state CDs with a photoluminescence quantum yield (PLQY) of 25%, which were successfully applied to WLD illumination. In recent years, our group obtained the highly stable CDs with PLQY of 47.09% by graphene oxide with high $sp^2$ conjugate structure, and solidified them by mixing with silane coupling agent KH-792 to obtain the fluorescent thin films with bright yellow light emission and high stability, and realized WLD illumination [13]. However, the phosphors for constructing high-quality LD devices should have not only high photothermal stability but also high PLQY, whereas the PLQY of solid-state CDs is still generally low (<60%). Hence, it is a challenge to realize the solid-state CDs phosphors with both high PLQY and high photothermal stability for LD devices.

Metal-organic frameworks (MOFs), as the protective matrices encapsulating functional materials, have the advantages of tunable structure, high porosity and high thermal stability [14]. The tight confinement in the cavities of MOFs can prevent the decomposition of functional materials at high temperatures, thus

* Corresponding author.
*E-mail address:* yangyongzhen@tyut.edu.cn (Y. Yang).

https://doi.org/10.1016/j.cclet.2023.109430
1001-8417/

enhancing the thermal stability of functional materials [15,16]. As a class of zeolite framework structured MOFs, zeolitic imidazolate framework-8 (ZIF-8) combines the advantages of both MOFs and zeolites, including simple preparation process, high thermal stability, high chemical stability, and easy structural modulation. Therefore, ZIF-8 can be utilized to encapsulate CDs to improve the thermal stability. In addition, the optical properties of CDs can be optimized by modulating the interaction between CDs and ZIF-8 surface functional groups, ultimately realizing the phosphors for WLD with high PLQY and high photothermal stability [17–19].

Here, the CDs@ZIF-8 with a stable network structure was obtained by employing ZIF-8 as a matrix to encapsulate CDs with amino functional groups. The as-prepared CDs@ZIF-8 exhibits an ultra-high PLQY of 81.17%, which mainly contributes to the formation of hydrogen bonds between CDs and ZIF-8 for enhancing the luminescence of CDs. In addition, the photothermal stability of CDs@ZIF-8 is significantly improved by effectively protecting CDs through confinement effect of ZIF-8. Further, the analysis confirm that the encapsulation structure plays a critical effect on the CDs@ZIF-8 morphology and photothermal performance. Finally, the prepared CDs@ZIF-8-based WLD exhibits color coordinates of (0.37, 0.33), a color temperature of 3762 K, and a color rendering index of 86, which promotes the development of low-cost, environmentally friendly solid-state phosphors for high-quality WLD devices.

The preparation process of CDs@ZIF-8 composites is shown in Fig. S1a (Supporting information). CDs were inserted and encapsulated within ZIF-8 in the synthesized process of ZIF-8, and the synthesized composite materials are called CDs@ZIF-8. In addition, in order to better reveal the interaction mechanism between CDs and ZIF-8, CDs and ZIF-8 were mixed by physical stirring to produce CDs/ZIF-8 composites (Fig. S1b in Supporting information), which are compared with CDs@ZIF-8. The morphology and size of CDs, ZIF-8, CDs@ZIF-8, and CDs/ZIF-8 were characterized by transmission electron microscopy (TEM) and scanning electron microscopy (SEM). As shown in Fig. S2a (Supporting information), CDs are *quasi*-spherical with an average particle size of about 2.12 nm. The high-resolution TEM (HRTEM) images show well-developed lattice fringes and a lattice spacing of 0.21 nm corresponding to the (100) plane of graphitic carbon, indicating a high degree of crystallization of CDs [20,21]. Figs. S2b and S3a (Supporting information) show the morphological structure of ZIF-8, which exhibits the rhombic dodecahedron with an average size of 83.72 nm. Figs. S2c, d and S3b, c (Supporting information) show TEM and SEM images of CDs@ZIF-8 and CDs/ZIF-8. It can be noticed that CDs/ZIF-8 is similar in size to ZIF-8, while CDs@ZIF-8 has smaller size and cross-linked in a network structure compared to ZIF-8. This is due to the fact that the CDs@ZIF-8 is synthesized by introducing CDs with abundant $-NH_2$ surface groups during the growth of ZIF-8, which can accelerate the deprotonation of ZIF-8 ligands, resulting in the rapid nucleation of ZIF-8 to form smaller-sized and randomly connected particles. This branched structure of ZIF-8 inhibits the rotation of its ligand and provides higher structural stability compared to conventional ZIF-8 [22]. Figs. 1a and b demonstrate the high angle angular dark field-scanning transmission electron microscopy (HADDF-STEM) images of CDs@ZIF-8 and CDs/ZIF-8, which can clearly observe the presence of CDs (as red circles). The particle size of CDs is larger than the pore size of conventional ZIF-8 (1.1 nm) [23], speculating that CDs are encapsulated within larger cavities stacked by ZIF-8 that grows around the CDs, rather than encapsulated within a single ZIF-8 pore [16,24]. In addition, a few CDs are also present on the ZIF-8 surface through electrostatic interactions, which can be confirmed by zeta potential tests (CDs: −4.1 mV, ZIF-8: 29.5 mV). It can be observed that part of the CDs adsorbed on the surface of ZIF-8 are detached by strong sonication (as yellow circles). For CDs/ZIF-8, CDs are adsorbed on the ZIF-8 surface by electrostatic interactions. Figs. 1c and d and Fig. S4 (Supporting information) exhibit the elemental mapping images of CDs@ZIF-8 and CDs/ZIF-8, and it can be found that the homogeneous distribution of Si elements of CDs demonstrates that the CDs are uniformly encapsulated or adsorbed inside and on ZIF-8 surface.

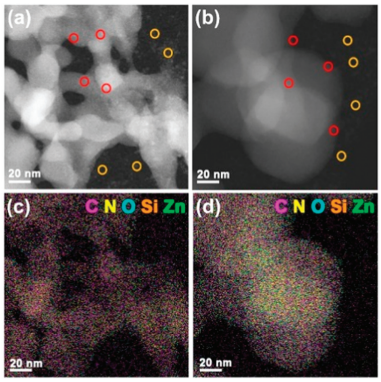


**Fig. 1.** HADDF-STEM image of CDs@ZIF-8 (a) and CDs/ZIF-8 (b). Element mapping of CDs@ZIF-8 (c) and CDs/ZIF-8 (d).

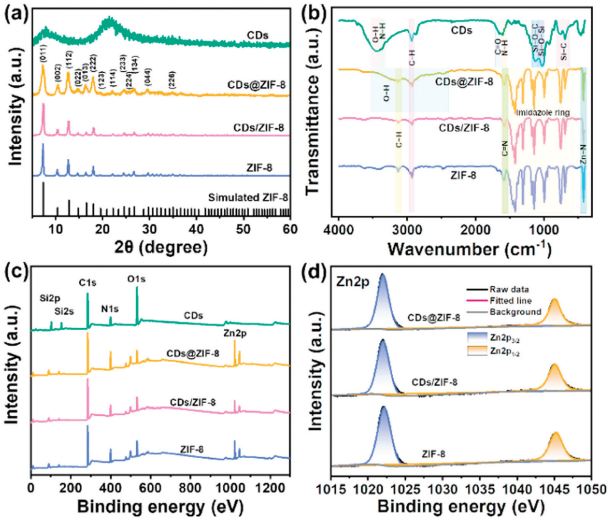


**Fig. 2.** The XRD (a), FTIR (b) and wide-range XPS (c) of CDs, ZIF-8, CDs@ZIF-8 and CDs/ZIF-8. (d) The high-resolution XPS spectra of Zn2p of CDs@ZIF-8, CDs/ZIF-8 and ZIF-8.

The microstructures of the products were characterized by X-ray diffraction (XRD), Fourier transform infrared spectroscopy (FTIR) and X-ray photoelectron spectroscopy (XPS). Fig. 2a demonstrates the XRD patterns of CDs@ZIF-8, CDs/ZIF-8, and ZIF-8. Their diffraction peaks at 7.3°, 10.4°, 12.7°, 14.7°, 16.4°, 18.0°, 19.4°, 22.0°, 24.5°, and 26.7° correspond to the (011), (002), (112), (022), (013), (222), (123), (114), (233), and (134), respectively. These diffraction peaks are consistent with the simulated peaks of ZIF-8 [25–27], indicating that the embedding of CDs did not hinder the formation of ZIF-8 in CDs@ZIF-8 and CDs/ZIF-8. The XRD pattern of CDs shows a broad diffraction peak at 21.5°, which is attributed to amorphous carbon [28]. Due to the weak intensity of the diffraction peaks of amorphous carbon itself and the overlap of the diffraction peaks of CDs with those of ZIF-8 at the (011) and (114) crystal planes, the CDs signals cannot be distinguished in CDs@ZIF-8 and CDs/ZIF-8.

The FTIR of CDs, CDs@ZIF-8, CDs/ZIF-8, and ZIF-8 are shown in Fig. 2b. The FTIR of CDs shows the absorption peaks located at 1604, 1650 and 2938 $cm^{-1}$ corresponding to the bending vibration of N–H, C=O and stretching vibration of C–H, respectively, suggesting that amide bonds are formed by dehydration condensation

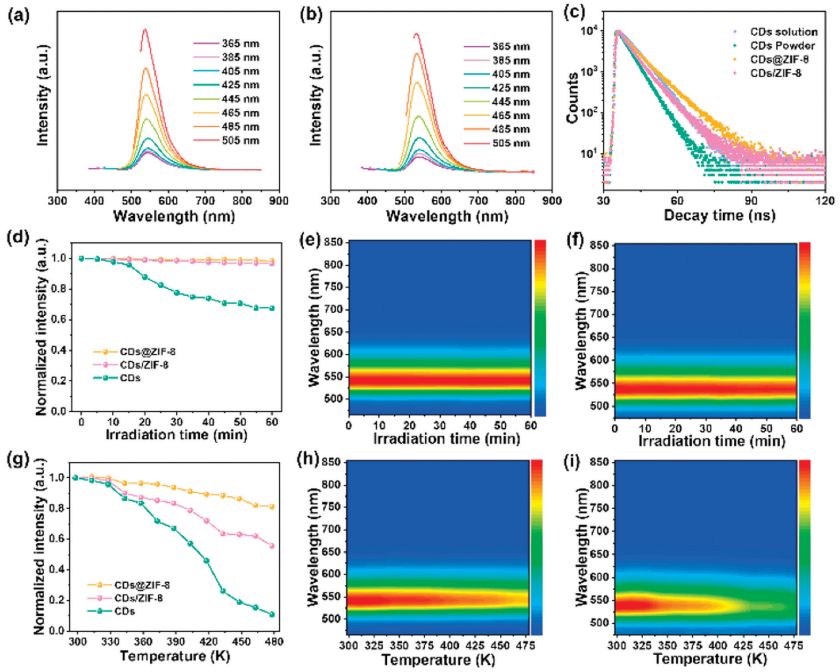


**Fig. 3.** PL spectra of CDs@ZIF-8 (a) and CDs/ZIF-8 (b) at different excitation wavelengths. (c) Fluorescence decay curves of CDs solution, CDs powder, CDs@ZIF-8 and CDs/ZIF-8. (d) Comparative diagrams of PL (450 nm excitation) intensity changes of CDs powder, CDs@ZIF-8 and CDs/ZIF-8 after different times of 450 nm laser irradiation. Fluorescence contour map of CDs@ZIF-8 (e) and CDs/ZIF-8 (f) *versus* time-dependent illumination (450 nm LD). (g) Comparative diagrams of PL (450 nm excitation) intensity changes of CDs powder, CDs@ZIF-8 and CDs/ZIF-8 at different temperatures. Fluorescence contour map of CDs@ZIF-8 (h) and CDs/ZIF-8 (i) *versus* temperature.

of the carbonyl group of erythrosine B (EB) and the amine group of (3-aminopropyl)trimethoxysilane (APTMs) [29]. The absorption peaks appearing at 695, 755, 1028, and 1127 $cm^{-1}$ correspond to the Si–C, Si–O–Si, and Si–O–C stretching vibrations, respectively [30,31], suggesting that silica-like structures can be formed by the hydrolyzation of APTMs during the reaction, in which the fluorophore is embedded by covalent bonding to increase the spatial positional resistance, endowing CDs with solid-state luminescent properties. After complexing CDs with ZIF-8, all the characteristic peaks of CDs are masked by ZIF-8. The absorption peak located at 421 $cm^{-1}$ is attributed to Zn–N stretching vibration. The absorption peak between 900 and 1350 $cm^{-1}$ is caused by the bending vibration of imidazole ring, and the absorption peaks between 1350 and 1500 $cm^{-1}$ originate from the stretching vibration of imidazole ring [32]. The peak located at 1585 $cm^{-1}$ belongs to the stretching vibration of the C=N bond. And 2930 and 3135 $cm^{-1}$ corresponds to the C–H stretching vibration of aliphatic and aromatic groups [33,34], respectively. Notably, the O–H absorption peak of CDs@ZIF-8 is blue-shifted compared to CDs and ZIF-8, suggesting that hydrogen bonding is formed between CDs and ZIF-8 [35].

Fig. 2c demonstrates the wide-range XPS survey scan spectra of CDs@ZIF-8 and CDs/ZIF-8. It can be seen that not only the peaks of C 1s, N 1s, and O 1s appear, but also the peaks of Si 2p and Zn 2p of typical ZIF-8 appear, respectively, implying that CDs were successfully complexed with ZIF-8. Further, the high-resolution XPS spectra of C, N, Zn, O and Si provided in Fig. 2d and Fig. S5 (Supporting information). The C 1s signal of CDs@ZIF-8 and CDs/ZIF-8 can be fitted with three peaks at 284.7 (C–C/C=C), 285.9 (C–N/C–O) and 288.7 eV (C=O/C=N). The N1s signal can be fitted with two peaks at 398.9 (C–N) and 400 eV (C=N/N–H). The O 1s signals at 530.6, 532 and 533.6 eV prove the presence of Si–O/Zn–O, C–O and C=O/O–H. Two peaks of Zn 2p spectrum are attributed to Zn $2p_{3/2}$ (1022 eV) and Zn $2p_{1/2}$ (1045 eV), which are in agreement with ZIF-8 [27]. In addition, a small amount of Si can be detected in the CDs@ZIF-8 and CDs/ZIF-8, which is fitted with two peaks at 101.3 (Si–C) and 102.3 eV (Si–O) [29], implying the presence of CDs. The above XPS results are consistent with the FTIR results.

In order to investigate the optical and thermal properties of CDs@ZIF-8 and CDs/ZIF-8, ultraviolet–visible absorption (UV–vis) spectra, photoluminescence spectra (PL), PLQY, and thermogravimetric curves (TG) were tested on CDs@ZIF-8 and CDs/ZIF-8. As shown in Figs. 3a and b and Figs. S6–S9 (Supporting information), the optimal excitation wavelength of CDs solution is 505 nm, and the optimal emission peak locates at 527 nm exhibiting green emission. Meanwhile, CDs solution exhibits excitation independence, narrow half-peak width (52 nm), and small stokes shift (28 nm), which is attributed to the single luminescent center (EB luminescent fluorophore), uniform particle size, and small non-radiative transition of CDs, respectively [36]. After CDs is dried to powder, the optimal emission peak of CDs is red-shifted to 546 nm, presenting yellow emission. This is attributed to a certain degree of overlap between the UV–vis spectra and PL spectra of CDs. The smaller spacing between CDs can cause solid-state resonance energy transfer, resulting in a red-shift in the emission wavelength of CDs and a decrease in the PLQY of CDs from 72.36% in the liquid state to 52.48% in the solid state [37]. As for CDs@ZIF-8 and CDs/ZIF-8, CDs are dispersed in ZIF-8 by internal encapsulation and surface adsorption, respectively. This can effectively expand the distance between CDs and attenuate the energy transfer within CDs, resulting in the blue-shifted emission wavelengths of composites compared to the solid-state CDs, which are 537 and 532 nm for CDs@ZIF-8 and CDs/ZIF-8, respectively [38]. The solid-state PLQY of CDs@ZIF-8 and CDs/ZIF-8 are 81.17% and 60.28%, respectively, among which CDs@ZIF-8 is the highest PLQY level of CDs-based solid-state yellow phosphors at present (Table S1 in Supporting information). It can be seen from Table S1 that the PLQY enhancement of CDs@ZIF-8 in this work is more obvious because the encapsulation structure of CDs@ZIF-8 suppresses the vibration and torsion of CDs and reduces the non-radiative transition process [39]. In Fig. S7c (Supporting information), CDs@ZIF-8 exhibits a small stokes shift of 30 nm, which also corroborates fewer

non-radiative transition in CDs@ZIF-8. In addition, the hydrogen bonding in CDs@ZIF-8 can enhance the degree of electron cloud delocalization, thus boosting the PLQY of CDs@ZIF-8 [40]. The fluorescence lifetimes of CDs@ZIF-8 and CDs/ZIF-8 are 7.23 and 5.67 ns, respectively, fitted from the fluorescence decay curves in Fig. 3c. Compared with CDs (solution: 5.66 ns, powder: 4.44 ns), the fluorescence lifetimes of composites increase, which further indicates that ZIF-8 plays a spatial limitation on CDs, inhibiting non-radiative transition [41]. Subsequently, the thermogravimetric (TG) curves of CDs@ZIF-8 and CDs/ZIF-8 are analyzed (Fig. S10 in Supporting information). CDs@ZIF-8 lose 4 wt% of weight between room temperature and 100 °C due to the volatilization of water molecules, and there is no obvious weight loss between 200 °C and 300 °C. After 300 °C, ZIF-8 ligand and the oxygen functional groups on the surface of CDs starts pyrolysis, and the pyrolysis of CDs@ZIF-8 is not complete until 800 °C. However, CDs/ZIF-8 starts to undergo thermal weight loss after 100 °C, and ZIF-8 framework rapidly collapses after 400 °C, and the whole weight loss process ends at 530 °C. The TG analysis result of CDs@ZIF-8 and CDs/ZIF-8 indicates that CDs@ZIF-8 with network structure has better thermal stability than CDs/ZIF-8. Afterwards, the photothermal stability of CDs, CDs@ZIF-8 and CDs/ZIF-8 are compared, as shown in Figs. 3d–i, Figs. S11 and S12 (Supporting information). The fluorescence intensity of CDs@ZIF-8 and CDs/ZIF-8 remains basically unchanged after continuous irradiation of CDs@ZIF-8 and CDs/ZIF-8 for 60 min with a 450 nm blue LD. In the test of thermal stability, the fluorescence intensity decay rates of samples are calculated according to the formula Eq. 1:

$$\text{Fluorescence decay rate} = \frac{A_0 - A_t}{A_0} \times 100\% \quad (1)$$

where $A_0$ is the fluorescence intensity of sample under 450 nm excitation at room temperature and $A_t$ is the fluorescence intensity of sample under 450 nm excitation at a certain temperature. The fluorescence intensity of CDs@ZIF-8, CDs/ZIF-8 and CDs are calculated to decay by 20%, 45% and 90% at 478 K, respectively (Fig. 3g and Figs. S12d–f in Supporting information). The reason that CDs@ZIF-8 enhancing the photothermal stability of CDs is mainly that ZIF-8 has a high thermal conductivity [42], which can accelerate the heat conduction from the continuous irradiation of LD, contributing to the heat dissipation of CDs. Moreover, ZIF-8 plays a role of encapsulation and confinement for CDs in CDs@ZIF-8, which can avoid the conformational change of CDs to denaturation when the temperature is increased [15]. Therefore, the thermal stability of CDs@ZIF-8 is better compared with that of CDs/ZIF-8.

In addition, the effect of different CDs additions (0.05, 0.1, 0.15 and 0.2 g) on the photothermal performance of CDs@ZIF-8 were investigated. As shown in Figs. S9c and S13 (Supporting information), the PLQY of CDs@ZIF-8 increases and then decreases with increased amount of CDs from 0.05 g to 0.2 g. The PLQY of CDs@ZIF-8 is maximal at 0.1 g of CDs. ZIF-8 matrix enables the CDs to be uniformly dispersed, increasing the distance between the CDs particles, effectively suppressing Förster resonance energy transfer and decreasing non-radiative transition [43]. Therefore, the PLQY of CDs@ZIF-8 is increased with an appropriate increase in the addition amount of CDs from 0.05 g to 0.1 g. When the CDs addition continues to increase, they may cluster, which can lead to a Förster resonance energy transfer between CDs, resulting in a decrease in the PLQY of CDs@ZIF-8, as well as inducing a redshift of the emission wavelength of CDs@ZIF-8 from 530 nm to 541 nm (Fig. 3a and Fig. S13 in Supporting information) [44]. The photothermal stability of CDs@ZIF-8 prepared with different addition of CDs was subsequently investigated. As shown in Figs. S12a, d, S14 and S15 (Supporting information), the fluorescence intensity of these CDs@ZIF-8 remain basically unchanged under blue LD irradiation for 60 min. However, the thermal stability of CDs@ZIF-8 decreases with the increased addition of CDs, and the initial decomposition temperature of CDs@ZIF-8 also decreases with the increased addition of CDs (Fig. S16 in Supporting information). In conclusion, with the increased addition of CDs, the PLQY of CDs@ZIF-8 increases and then decreases, and the stability decreases. The CDs@ZIF-8 prepared with 0.1 g of CDs is determined to exhibit the best performance in this research.

In short, the CDs@ZIF-8 prepared with encapsulated structure shows a better optical and thermal performance than CDs/ZIF-8, which not only has a high PLQY of up to 81.17%, but also possesses excellent optical, thermal and photothermal stability. Three reasons are summarized as follows. Firstly, ZIF-8 encapsulating CDs is beneficial for the uniform dispersion of CDs, increasing the distance between CDs particles, effectively suppressing Förster resonance energy transfer, and reducing non-radiative transition. Secondly, hydrogen bonds are formed between the free N—H on the surface of ZIF-8 and the O—H on the surface of CDs (Fig. 4a), which can greatly enhance the degree of electron cloud delocalization and increase the concentration of photogenerated electrons, thus significantly improving the fluorescence emission intensity. Finally, ZIF-8 plays a binding effect on the encapsulated CDs, and the vibration and torsion of CDs can be suppressed relying on the bonding interactions between CDs and ZIF-8, which both reduce the non-radiative transition of materials and prevent CDs from decomposing at high temperature.

The CDs@ZIF-8 with high PLQY and photothermal stability as yellow phosphor combined with red fluoride phosphor was applied to WLD devices. Fig. 4b shows the white light emission spectrum of WLD device at an operating voltage of 3.8 V. The emission peak located at 450 nm belongs to blue LD, while the emis-

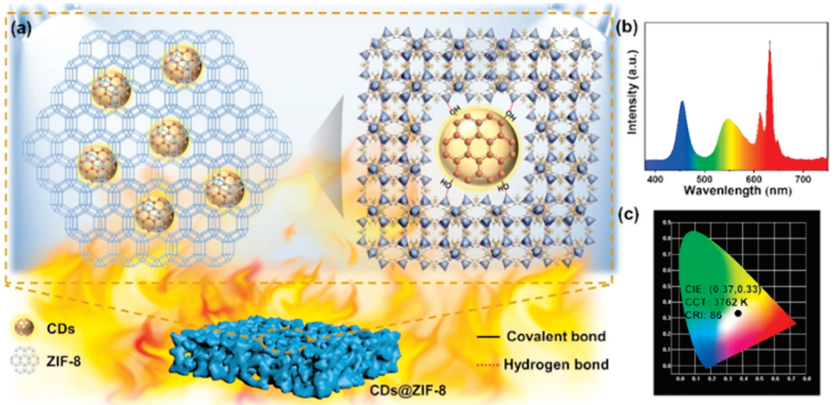


**Fig. 4.** (a) The internal structure diagram of CDs@ZIF-8. (b) The emission spectra of WLD device. (c) The color coordinate of the WLD device.

sion peak located near 540 nm is attributed to CDs@ZIF-8, and the emission peak of red fluoride phosphor is around 632 nm. The WLD device has a color coordinate of (0.37, 0.33), a color temperature of 3762 K and a color rendering index of 86 (Fig. 4c). Subsequently, the performance of the WLD device was tested at 5 min intervals under 200 min operating duration, as shown in Fig. S17 (Supporting information), the emission spectra, color coordinate, color rendering index, and color temperature of WLD device basically remain unchanged under the continuous operating conditions within 200 min, indicating that the WLD device has excellent stability based on the stabilized CDs@ZIF-8 fluorescent materials, which demonstrates the superior light application prospects of CDs@ZIF-8.

In summary, the solid-state yellow CDs@ZIF-8 phosphors, with PLQY of 81.17% and stable fluorescence performance under continuous light (60 min) and 478 K, were synthesized by inserting CDs inside ZIF-8 during the synthesis of ZIF-8. Morphological and structural analyses show that CDs@ZIF-8 has a network cross-linking structure that can inhibit the rotation of the ZIF-8 ligand, resulting in higher structural stability. Photothermal performance analysis further reveals that the high PLQY and excellent photothermal stability of CDs@ZIF-8 are mainly attributed to the bonding interactions between CDs and ZIF-8, which can inhibit the vibration and torsion of the CDs to play a confinement effect on the CDs. Finally, the WLD device, which was fabricated by CDs@ZIF-8 as phosphor combining with 450 nm blue LD, shows good white-light illumination performance with color coordinates of (0.37, 0.33), color temperature of 3762 K, and color rendering index of 86. This work realizes the preparation of solid-state yellow light environment-friendly phosphor with high PLQY and high photothermal stability for the first time through the ZIF-8 encapsulation strategy, which has great significance for the realization of high-efficiency WLD.

## Declaration of competing interest

The authors declare that they have no known competing financial interests or personal relationships that could have appeared to influence the work reported in this paper.

## Acknowledgments

This work is financially supported by the Foundational Research Project of Shanxi Province (No. 20210302123164), Shanxi-Zheda Institute of Advanced Materials and Chemical Engineering (Nos. 2022SX-TD012, 2021SX-TD012), and Shanxi Scholarship Council of China (No. 2020–051). The authors acknowledge the assistance of Instrumental Analysis Center of Taiyuan University of Technology.

## Supplementary materials

Supplementary material associated with this article can be found, in the online version, at doi:10.1016/j.cclet.2023.109430.

## References

[1] S.X. Li, Q.Q. Zhu, D.M. Tang, et al., J. Mater. Chem. C 4 (2016) 8648–8654.
[2] C. Cozzan, G. Lheureux, N. O'Dea, et al., ACS Appl. Mater. Interfaces 10 (2018) 5673–5681.
[3] A. Neumann, J.J. Wierer, W. Davis, et al., Opt. Express 19 (2011) A982–A990.
[4] J. Xu, A. Thorseth, C. Xu, et al., J. Lumin. 212 (2019) 279–285.
[5] C.L. Xia, S.J. Zhu, T.L. Feng, et al., Adv. Sci. 6 (2019) 1901316.
[6] X.T. Zheng, A. Ananthanarayanan, K.Q. Luo, et al., Small 11 (2015) 1620–1636.
[7] B. Unnikrishnan, C.W. Wu, I.W.P. Chen, et al., ACS Sustain. Chem. Eng. 4 (2016) 3008–3016.
[8] Y.S. Ma, Y. Cen, M. Sohail, et al., ACS Appl. Mater. Interfaces 9 (2017) 33011–33019.
[9] M.Y. Fang, B.Y. Wang, X.L. Qu, et al., Chin. Chem. Lett. 35 (2024) 108423.
[10] X. Yang, X. Li, B.Y. Wang, et al., Chin. Chem. Lett. 33 (2022) 613–625.
[11] B. Chen, J.C. Feng, J. Phys. Chem. C 119 (2015) 7865–7872.
[12] Z.J. Zhou, P.F. Tian, X.Y. Liu, et al., Adv. Sci. 5 (2018) 1800369.
[13] P.Y. He, S. Yang, X.H. Liu, et al., J. Lumin. 238 (2021) 118275.
[14] Y.Q. Xue, S.S. Zheng, H.G. Xue, et al., J. Mater. Chem. A 7 (2019) 7301–7327.
[15] K. Liang, R. Ricco, C.M. Doherty, et al., Nat. Commun. 6 (2015) 7240.
[16] R. Murty, M.K. Bera, I.M. Walton, et al., J. Am. Chem. Soc. 145 (2023) 7323–7330.
[17] Z. Wang, X.D. Jin, L.P. Yan, et al., Microchim. Acta 190 (2023) 28.
[18] H.Y. Zhang, B.L. Wang, X.W. Yu, et al., Angew. Chem. Int. Ed. 59 (2020) 19390–19402.
[19] B.Y. Wang, G.I.N. Waterhouse, S.Y. Lu, Trends Chem. 5 (2023) 76–87.
[20] Z.S. Yan, T. Chen, L.P. Yan, et al., Adv. Sci. 10 (2023) 2206386.
[21] Q. Li, J.B. Fan, H.K. Mu, et al., Chin. Chem. Lett. 35 (2023) 108947.
[22] H. Lee, W.S. Chi, M.J. Lee, et al., Adv. Funct. Mater. 32 (2022) 2207775.
[23] N. Hara, M. Yoshimune, H. Negishi, et al., J. Membr. Sci. 450 (2014) 215–223.
[24] J.C. Liu, H.Y. Zhang, N. Wang, et al., ACS Mater. Lett. 1 (2019) 58–63.
[25] K.S. Park, Z. Ni, A.P. Cote, et al., Proc. Natl. Acad. Sci. U. S. A. 103 (2006) 10186–10191.
[26] R. Banerjee, A. Phan, B. Wang, et al., Science 319 (2008) 939–943.
[27] L. Zhou, N. Li, G. Owens, et al., Chem. Eng. J. 362 (2019) 628–637.
[28] Y. Wang, X. Liu, X.Y. Han, et al., Nat. Commun. 11 (2020) 2531.
[29] Y.H. Wu, L.X. Zhao, X.Y. Cao, et al., Carbon 207 (2023) 77–85.
[30] L.H. Bai, H.X. Yan, Y.B. Feng, et al., Chem. Eng. J. 373 (2019) 963–972.
[31] Y.Q. Zhang, M.Y. Li, S.Y. Lu, et al., Small 19 (2023) 2206080.
[32] S.C. Wu, Y. Chen, X. Yan, et al., Chem. Eng. J. 442 (2022) 136139.
[33] L. Lin, H.O. Liu, X.F. Zhang, et al., Chem. Eng. J. 328 (2017) 124–132.
[34] V. Vatanpour, A. Yuksekdag, M. Agtas, et al., Carbohydr. Polym. 299 (2023) 120230.
[35] C.W. Zhang, F.Y. Li, J.F. Li, et al., J. Clean Prod. 185 (2018) 357–365.
[36] J.Y. Chen, W.R. Liu, Y.J. Li, et al., Chem. Eng. J. 428 (2022) 131168.
[37] Y.H. Chen, M.T. Zheng, Y. Xiao, et al., Adv. Mater. 28 (2016) 312–318.
[38] X. Gong, S.Y. Zheng, X.J. Zhao, et al., Nano Energy 101 (2022) 107617.
[39] J.C. Liu, N. Wang, Y. Yu, et al., Sci. Adv. 3 (2017) 1603171.
[40] M. Zhang, C.J. Zheng, K. Wang, et al., Adv. Funct. Mater. 31 (2021) 2010100.
[41] Y.T. Lu, S. Wang, K.L. Yu, et al., Microporous Mesoporous Mater. 319 (2021) 111062.
[42] J. Huang, A.R. Fan, X.X. Xia, et al., ACS Nano 14 (2020) 14100–14107.
[43] H.L. Wang, L. Ai, H.Q. Song, et al., Adv. Funct. Mater. 33 (2023) 2303756.
[44] J.X. Ni, X.L. Huang, Y.B. Bai, et al., Adv. Compos. Hybrid Mater. 5 (2022) 1865–1875.